2017

Regulation of neurite morphogenesis by interaction between R7 regulator of G protein signaling complexes and G protein subunit Gα13

Stephanie L. Scherer
Washington University School of Medicine in St. Louis

Matthew D. Cain
Washington University School of Medicine in St. Louis

Stanley M. Kanal
Washington University School of Medicine in St. Louis

Kevin M. Kaltenbronn
Washington University School of Medicine in St. Louis

Kendall J. Blumer
Washington University School of Medicine in St. Louis

Regulation of neurite morphogenesis by interaction between R7 regulator of G protein signaling complexes and G protein subunit $G\alpha_{13}$

Received for publication, December 9, 2016, and in revised form, April 19, 2017 Published, Papers in Press, April 21, 2017, DOI 10.1074/jbc.M116.771923

Stephanie L. Scherer, Matthew D. Cain, Stanley M. Kanai, Kevin M. Kaltenbronn, and Kendall J. Blumer[1]

From the Department of Cell Biology and Physiology, Washington University School of Medicine, St. Louis, Missouri 63110

Edited by Henrik G. Dohlman

The R7 regulator of G protein signaling family (R7-RGS) critically regulates nervous system development and function. Mice lacking all R7-RGS subtypes exhibit diverse neurological phenotypes, and humans bearing mutations in the retinal R7-RGS isoform RGS9-1 have vision deficits. Although each R7-RGS subtype forms heterotrimeric complexes with $G\beta_5$ and R7-RGS-binding protein (R7BP) that regulate G protein-coupled receptor signaling by accelerating deactivation of $G_{i/o}$ α-subunits, several neurological phenotypes of R7-RGS knock-out mice are not readily explained by dysregulated $G_{i/o}$ signaling. Accordingly, we used tandem affinity purification and LC-MS/MS to search for novel proteins that interact with R7-RGS heterotrimers in the mouse brain. Among several proteins detected, we focused on $G\alpha_{13}$ because it had not been linked to R7-RGS complexes before. Split-luciferase complementation assays indicated that $G\alpha_{13}$ in its active or inactive state interacts with R7-RGS heterotrimers containing any R7-RGS isoform. LARG (leukemia-associated Rho guanine nucleotide exchange factor (GEF)), PDZ-RhoGEF, and p115RhoGEF augmented interaction between activated $G\alpha_{13}$ and R7-RGS heterotrimers, indicating that these effector RhoGEFs can engage $G\alpha_{13}$·R7-RGS complexes. Because $G\alpha_{13}$/R7-RGS interaction required R7BP, we analyzed phenotypes of neuronal cell lines expressing RGS7 and $G\beta_5$ with or without R7BP. We found that neurite retraction evoked by $G\alpha_{12/13}$-dependent lysophosphatidic acid receptors was augmented in R7BP-expressing cells. R7BP expression blunted neurite formation evoked by serum starvation by signaling mechanisms involving $G\alpha_{12/13}$ but not $G\alpha_{i/o}$. These findings provide the first evidence that R7-RGS heterotrimers interact with $G\alpha_{13}$ to augment signaling pathways that regulate neurite morphogenesis. This mechanism expands the diversity of functions whereby R7-RGS complexes regulate critical aspects of nervous system development and function.

Regulator of G protein signaling (RGS)[2] proteins regulate the amplitude and kinetics of G protein-coupled receptor signaling by functioning in part as GTPase-activating proteins (GAPs) that accelerate the rate that G protein α-subunits hydrolyze GTP to GDP (1). Among ~30 mammalian proteins containing an RGS domain, the R7 regulator of G protein signaling family (R7-RGS), consisting of RGS6, RGS7, RGS9, and RGS11, is particularly important. R7-RGS proteins are highly expressed in the nervous system and exhibit GAP activity *in vitro* only for $G\alpha_{i/o}$ (2–7). Humans bearing mutations in the retinal RGS9-1 isoform exhibit a vision deficit termed bradyopsia (8), and mice lacking selected or all R7-RGS proteins exhibit various neurological phenotypes manifested by impairment of perinatal viability, weight gain, retina structure and function, neurobehavioral development, motor coordination, cerebellar and hippocampal development, and analgesic response to opioids (9–12), thereby establishing these regulators as crucial players in neurological development and function.

Evidence suggests that R7-RGS proteins have diverse mechanistic functions beyond serving as $G\alpha_{i/o}$-specific GAPs. First, in contrast to several other classes of RGS proteins that are GAPs for $G_{i/o}$ α-subunits (13), R7-RGS proteins are structurally complex. Each R7-RGS isoform possesses N-terminal dishevelled, Egl-10, and pleckstrin (DEP), DEP helical extension (DHEX), and G protein γ-like (GGL) domains followed by a C-terminal RGS domain that is necessary and sufficient for GAP activity. The GGL domain binds the most diverged member of the $G\beta$ family, $G\beta_5$ (4, 14), to form obligate heterodimeric complexes structurally similar to classical $G\beta\gamma$ dimers (15). The DEP domain interacts with either of two SNARE-like membrane anchor proteins (16–21), R7-RGS-binding protein (R7BP) and RGS9 anchor protein (R9AP), to form R7-RGS heterotrimers. Whereas R9AP is a transmembrane protein local-

This work was supported by National Institutes of Health Grants GM044592 and HL075632 (to K. J. B.). The authors declare that they have no conflicts of interest with the contents of this article. The content is solely the responsibility of the authors and does not necessarily represent the official views of the National Institutes of Health.

This article contains supplemental Table 1.

[1] To whom correspondence should be addressed: Box 8228, Washington University School of Medicine, 660 S. Euclid Ave., St. Louis, MO 63110. Tel.: 314-362-1668; Fax: 314-362-7463; E-mail: kblumer@wustl.edu.

[2] The abbreviations used are: RGS, regulator of G protein signaling; R7-RGS, R7 regulator of G protein signaling family; R7BP, R7-RGS-binding protein; $G\beta_5$, G protein β-subunit isoform 5; DSS, disuccinimidyl suberate; CBG, click beetle green luciferase; CBGN, N-terminal fragment of click beetle green luciferase; CBGC, C-terminal fragment of click beetle green luciferase; TAP, tandem affinity purification; PTX, pertussis toxin; LPA, lysophosphatidic acid; GAP, GTPase-activating protein; N2a, Neuro2a; GEF, guanine nucleotide exchange factor; LARG, leukemia-associated Rho guanine nucleotide exchange factor; DEP, disheveled, Egl-10, and pleckstrin; DHEX, DEP helical extension; GGL, G protein γ-like; R9AP, RGS9 anchor protein; RH, RGS homology; HPRT, hypoxanthine-guanine phosphoribosyltransferase; PGK-Neo, phosphoglycerate kinase-neomycin resistance; MoPRP, mouse prion protein; PDL, poly-D-lysine; DPBS, Dulbecco's PBS; SF, Strep/FLAG.

ized to photoreceptor disk membranes, R7BP is reversibly and dynamically palmitoylated to regulate plasma membrane localization of R7-RGS heterotrimers throughout much of the nervous system (17, 22–24). Second, as shown in *Caenorhabditis elegans*, the N-terminal DEP/DHEX domain rather than the RGS domain of R7-RGS proteins determines which neurological processes mediated by distinct G proteins are regulated (25). Third, RGS7·Gβ_5 and RGS9-2·Gβ_5 complexes, respectively, can attenuate G_q-coupled type 3 muscarinic or $G_{i/o}$-coupled type 3 dopamine receptors by GAP-independent mechanisms (19, 21), similar to other structurally complex RGS proteins that serve as multifunctional regulators, integrators, and/or effectors in signaling networks (26, 27). Lastly, RGS6 can scaffold DNA methyltransferase 1 to the acyltransferase Tip60 to promote DNA methyltransferase 1 degradation in response to Ras activation in mouse embryonic fibroblasts (28, 29).

Despite such evidence, whether the membrane anchor R7BP is required for functions of R7-RGS complexes other than G$\alpha_{i/o}$-specific GAP activity has not been investigated. Here we have addressed this question by using a proteomics approach to identify proteins that interact with R7BP-bound R7-RGS complexes in mouse brain. Our results expand understanding of R7BP-bound R7-RGS complexes by indicating that they facilitate Gα_{13} signaling to regulate neurite morphogenesis.

Results

RGS7, Gβ_5, and R7BP form macromolecular complexes larger than simple heterotrimers in neuronal cells

If R7BP-bound R7-RGS proteins have novel functions, they would be expected to participate in novel protein-protein interactions. Accordingly, we investigated whether RGS7, Gβ_5, and R7BP exist in macromolecular complexes larger than simple heterotrimers in living cells. We used Neuro2a (N2a) cells endogenously expressing RGS7 and Gβ_5 and stably transfected with N-terminally FLAG-tagged R7BP at physiologically normal levels (5) that were treated with vehicle or disuccinimidyl suberate (DSS), a cell-permeable, amine-reactive cross-linker. Cell lysates were immunoprecipitated with FLAG antibody, resolved via SDS-PAGE, and immunoblotted to detect Gβ_5, the obligate core subunit of all R7-RGS complexes. As expected if additional proteins associate with R7-RGS heterotrimers, this approach detected several distinct species with relative molecular weights larger than R7-RGS heterotrimers (Fig. 1*A*). These experiments also detected non-cross-linked Gβ_5 and cross-linked R7-RGS·Gβ_5·FLAG-R7BP heterotrimers (Fig. 1*A*). These results are consistent with an independent study in which complexes containing R7BP were detected in lysates of transfected HEK293T cells and mouse brain lysates cross-linked with paraformaldehyde (30).

Generation of transgenic mice expressing tandem affinity purification (TAP)-tagged R7BP

To identify potentially novel proteins that associate with R7BP-containing R7-RGS heterotrimers, we isolated these complexes from brain tissue by affinity purification and identified proteins recovered with these complexes by liquid chromatography-coupled tandem mass spectrometry (LC-MS/MS). This approach was motivated by prior studies showing that the membrane anchor R9AP and transducin α-subunits co-purify with RGS9-1·Gβ_5 heterodimers in photoreceptor membranes (20) and that an orphan G protein-coupled receptor (GPR158) associates with RGS7·Gβ_5 heterodimers in brain lysates (18, 31). However, our approach was novel because it identified proteins that associate with heterotrimers containing any R7-RGS isoform, Gβ_5, and R7BP.

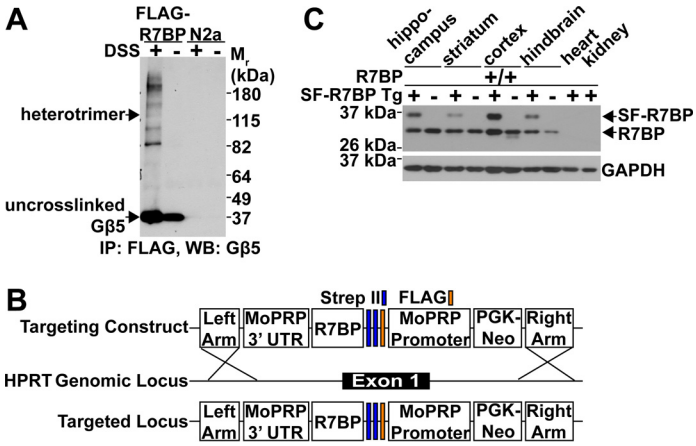

Figure 1. Generation of SF-R7BP transgenic mice to identify novel proteins that interact with R7-RGS heterotrimers. *A*, live-cell chemical cross-linking. N2a cells lacking or stably expressing 3xFLAG-R7BP were treated with DSS followed by immunoprecipitation (*IP*) of R7BP-containing cross-linked complexes. Immunoprecipitation eluates were separated by SDS-PAGE and immunoblotted for Gβ_5 (shown), RGS7, and R7BP (not shown). The band corresponding to R7-RGS heterotrimers was indicated by detection with Gβ_5, RGS7, and R7BP antibodies. Data shown are representative of three independent experiments. *B*, SF-R7BP transgenic mice were generated by targeting SF-R7BP in reverse orientation to the *Hprt* locus on the X chromosome as described under "Experimental procedures." SF-R7BP expression was by the neuron-specific MoPRP. *C*, Western blot (*WB*) analysis of lysates from the indicated brain regions and other organs from non-transgenic control and SF-R7BP transgene-positive male mice. Wild-type untagged R7BP was expressed from its endogenous locus. Data are representative of three independent SF-R7BP transgenic lines.

We developed a TAP strategy in which the FLAG-StrepII-StrepII tag (32) was appended to the N terminus of R7BP (SF-R7BP; Fig. 1*B*) and generated transgenic mice expressing this protein specifically in neurons. This was accomplished by driving SF-R7BP expression from the mouse prion promoter upon integration of the transgene in single copy at the X-linked *Hprt* locus (33, 34) (Fig. 1*B*). As indicated by immunoblotting with anti-R7BP antibodies, SF-R7BP and endogenously expressed R7BP were expressed similarly in various brain regions and were undetectable in heart and kidney (Fig. 1*C*). Importantly, SF-R7BP was not overexpressed relative to endogenous R7BP, reducing concern of identifying biologically irrelevant protein-protein interactions due to overexpression. SF-R7BP protein expression profiles were similar in three independently derived transgenic lines, all of which were used for TAP experiments. In all subsequent experiments, SF-R7BP-expressing adult male mice were used to avoid potentially mosaic expression of SF-R7BP due to X chromosome inactivation in females.

Tandem affinity purification and LC-MS/MS analysis of R7BP-containing protein complexes

R7BP-containing protein complexes were isolated from the combined lysates of three SF-R7BP adult male mouse brains as detailed under "Experimental procedures." The purification

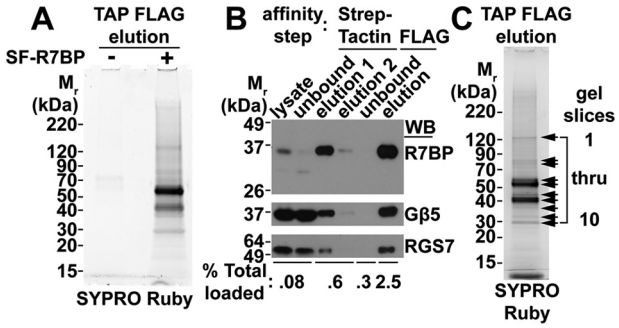

Figure 2. TAP of SF-R7BP and interacting proteins from mouse brain. *A*, assessing nonspecific background in TAP experiments. TAP was performed as described under "Experimental procedures" using detergent-solubilized brain homogenates from either three SF-R7BP-positive or three SF-R7BP-negative male mice as indicated. The final eluates were separated by SDS-PAGE, and proteins were visualized by SYPRO Ruby staining. *B*, Western blot (*WB*) analysis of SF-R7BP, Gβ_5, and RGS7 for each step of the TAP protocol. *C*, SYPRO Ruby-stained gel of the TAP eluate from three SF-R7BP-positive mouse brains. *Arrows* indicate regions of the gel that were excised and analyzed by LC-MS/MS. Mass spectrometry data summarized in Table 1 and supplemental Table 1 are organized by gel slice numbers indicated in this panel.

procedure was optimized to achieve low nonspecific protein binding as indicated by SYPRO Ruby staining of TAP eluates from control non-transgenic mice relative to SF-R7BP transgenic mice (Fig. 2*A*). Moreover, the purification conditions preserved R7-RGS heterotrimers as indicated by immunoblotting showing that Gβ_5 and RGS7 co-purified with SF-R7BP (Fig. 2*B*).

Proteins that co-purified with R7-RGS heterotrimers were identified by resolving TAP FLAG eluates on SDS-PAGE, excising and extracting SYPRO Ruby-stained gel bands, and digesting with Glu-C and trypsin (Fig. 2*C*). The resulting peptides were sequenced by LC-MS/MS, and the corresponding proteins were identified as described under "Experimental procedures." Detailed peptide and protein identification data are summarized in Table 1 and supplemental Table 1. As expected, SF-R7BP (denoted in Table 1 as Rgs7bp protein), Gβ_5, and three of the four R7-RGS isoforms (RGS11 was not detected, presumably due to limited expression in brain) were identified (Table 1 and supplemental Table 1). Gα_o, which is a substrate for the GAP function of R7-RGS heterotrimers, also was identified with high confidence.

Gα_{13} is a novel binding partner of R7-RGS heterotrimers

Gα_{13} was identified with high confidence in our LC-MS/MS analysis of proteins that co-purified with SF-R7BP-bound R7-RGS complexes (Table 1 and supplemental Table 1). Similarly, Gα_{13} was identified in TAP-LC-MS/MS experiments using N2a cells expressing SF-R7BP (data not shown). Although unique peptides diagnostic of other Gα isoforms or classical G$\beta\gamma$ subunits were not detected, we cannot exclude that these proteins were present in R7-RGS complexes bound to SF-R7BP.

Recovery of Gα_{13} was intriguing for two reasons. First, Gα_{13} is not a substrate for the GAP function of R7-RGS heterotrimers that is specific *in vitro* for G$\alpha_{i/o}$ subunits (2–4). Therefore, co-purification of Gα_{13} with R7-RGS complexes suggested that R7-RGS heterotrimers potentially influence the function of this Gα subunit by GAP-independent mechanisms. Second, mice deficient in all R7-RGS heterotrimers due to knock-out of the shared obligate subunit Gβ_5 have abnormal dendritic morphology as seen in retinal ON-bipolar and Purkinje neurons (10, 11). Because Gα_{13} is a well established regulator of the actin cytoskeleton, which regulates dendritic morphogenesis, a functional relationship between R7-RGS heterotrimers and Gα_{13} might account in part for the dendritic morphology phenotypes of G$\beta_5^{-/-}$ mice. Accordingly, the remainder of the present study focused on the interaction between R7-RGS heterotrimers and Gα_{13}.

To provide independent evidence whether Gα_{13} can associate with R7-RGS heterotrimers, we adopted split-luciferase complementation assays to assess protein-protein interactions in living cells (35, 36). Because split-luciferase complementation apparently had not been used before with Gα subunits, we first determined whether this technique is appropriate for our purposes. We inserted the N-terminal fragment of click beetle green luciferase (CBGN; Ref. 36) into the αB-αC loop of the helical domain in wild-type and constitutively active (*i.e.* GTPase-defective Gln → Leu (Q/L) mutants) forms of Gα_q and Gα_{13} because insertion of GFP at this site preserves Gα function (37). The C-terminal fragment of click beetle green luciferase (CBGC) was fused to the N termini of the following proteins: RGS2 (CBGC-RGS2), a GAP for Gα_q but not Gα_{13}; the RH-RGS domain of LARG (CBGC-LARG·RGS), a GAP for Gα_{13} but not Gα_q; and Gβ_1 (CBGC-Gβ_1). These constructs were used to determine whether split-luciferase complementation detects specific and activity-dependent interaction between Gα_q or Gα_{13} and their cognate binding partners in intact cells.

This expectation was confirmed by results of luciferase assays performed with HEK293 cells co-transfected with various combinations of split luciferase-tagged proteins (Fig. 3*A*). Wild-type CBGN-tagged Gα_q or Gα_{13} complemented strongly with CBGC-Gβ_1 co-transfected with Gγ_2. Constitutively active Gα_{13}(Q/L)-CBGN complimented strongly with CBGC-LARG·RGS but not CBGC-RGS2. Likewise, constitutively Gα_q(Q/L)-CBGN complemented strongly with CBGC-RGS2 but not CBGC-LARG·RGS. Wild-type Gα_{13}-CBGN and Gα_q-CBGN complemented insignificantly, respectively, with CBGC-LARG·RGS and CBGC-RGS2. Thus, split-luciferase complementation detected specific protein-protein interactions determined by Gα subunit identity and activation state.

Split-luciferase complementation then was used to study interaction between Gα_{13} and R7-RGS heterotrimers and to determine whether this interaction is affected by the activity state of Gα_{13}. In these experiments, HEK293 cells were co-transfected with CBGC-FLAG-Gβ_5, HA-RGS7 with or without FLAG-R7BP, various Gα-CBGN constructs, and *Renilla* luciferase as a transfection control. When co-expressed with HA-RGS7 and FLAG-R7BP, CBGC-FLAG-Gβ_5 strongly complemented with either wild-type or constitutively active Gα_{13}-CBGN but not with wild-type or constitutively active Gα_q-CBGN (Fig. 3*B*). These results confirmed that R7-RGS heterotrimers and Gα_{13} interact in a specific manner rather than by nonspecific collisional interaction within the plane of the plasma membrane and indicated that this interaction is independent of Gα_{13} activation. These interactions required the

Table 1

Subset of proteins identified by LC-MS/MS analysis of TAP fractions

Protein bands marked with an *arrow* in Fig. 2*C* were analyzed by LC-MS/MS to identify proteins that co-purified with SF-R7BP from transgenic mouse brain. Peptide identifications were accepted if they could be established at greater than 80% probability by the Scaffold local false discovery rate algorithm. All proteins shown here have at least a 99% protein identification (ID) probability as determined using the Protein Prophet algorithm and at least two exclusive unique peptides assigned. Tabulated are protein identification information for R7BP (Rgs7bp protein); R7-RGS family members; and Gβ_5, Gα_o, and a novel interacting protein, Gα_{13}. See supplemental Table 1 for a complete list of all proteins identified and peptide sequence information.

Gel slice	Protein name	Accession number	Protein ID probability	Exclusive unique peptides	Exclusive unique spectra	Total spectra	Sequence coverage
			%				%
6	Rgs7bp protein (*Mus musculus*)	gi 111600355	100.00	3	4	12	19.50
7	Rgs7bp protein (*M. musculus*)	gi 111600355	100.00	3	4	87	13.60
8	Rgs7bp protein (*M. musculus*)	gi 111600355	100.00	2	3	73	22.60
2	Regulator of G-protein signaling 9 isoform 1 (*M. musculus*)	gi 146134422	100.00	5	7	21	24.30
3	Regulator of G-protein signaling 9 isoform 1 (*M. musculus*)	gi 146134422	100.00	4	4	14	18.70
4	Regulator of G-protein signaling 6 (*M. musculus*)	gi 29789076	100.00	6	8	15	20.30
5	Regulator of G-protein signaling 6 (*M. musculus*)	gi 29789076	100.00	7	9	11	18.60
4	Regulator of G-protein signaling 7 (*M. musculus*)	gi 312222673	100.00	9	11	26	21.70
5	Regulator of G-protein signaling 7 (*M. musculus*)	gi 312222673	99.90	5	6	12	12.30
6	Guanine nucleotide-binding protein subunit β_5 isoform 2 (*M. musculus*)	gi 41281679	100.00	4	5	5	5.67
7	Guanine nucleotide-binding protein subunit β_5 isoform 2 (*M. musculus*)	gi 41281679	100.00	17	20	25	26.10
8	Guanine nucleotide-binding protein subunit β_5 isoform 2 (*M. musculus*)	gi 41281679	100.00	5	6	6	8.22
9	Guanine nucleotide-binding protein subunit β_5 isoform 2 (*M. musculus*)	gi 41281679	100.00	3	4	4	5.67
10	Guanine nucleotide-binding protein subunit β_5 isoform 2 (*M. musculus*)	gi 41281679	100.00	2	3	3	5.10
7	Guanine nucleotide-binding protein subunit α_{13} (*M. musculus*)	gi 89001109	100.00	2	2	3	10.10
7	Guanine nucleotide-binding protein G_o subunit α isoform B (*M. musculus*)	gi 164607137	99.00	2	2	3	7.63

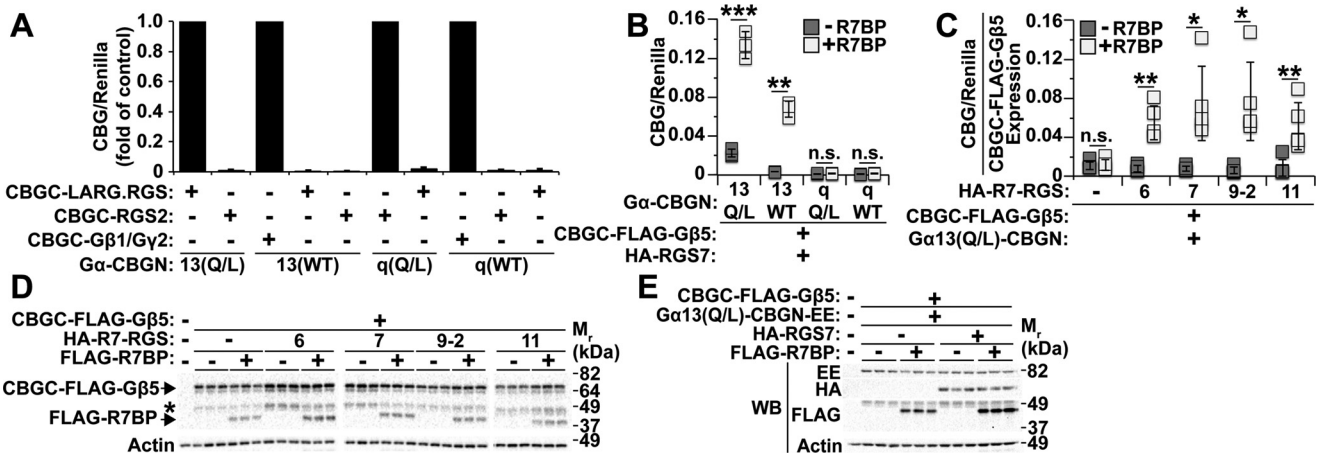

Figure 3. R7BP is required to detect interaction between Gα_{13} and R7-RGS complexes containing any R7-RGS family member. *A*, proof of concept that split-luciferase complementation detects protein-protein interactions specific for Gα subunit identity and activity state. Data are represented as the -fold difference in normalized split-luciferase signal relative to the positive control for each Gα-CBGN construct. Data shown are the average of three independent experiments. *B*, split-luciferase complementation between the indicated Gα-CBGN proteins and CBGC-Gβ_5·RGS7 with or without R7BP. Each *box* represents a data point from one of three independent experiments. *C*, split-luciferase complementation between Gα_{13}(Q/L)-CBGN and CBGC-3xFLAG-Gβ_5 co-expressed with each R7-RGS isoform with or without R7BP. Luciferase signals were normalized to the level of CBGC-3xFLAG-Gβ_5 expression determined by immunoblotting. Each *box* represents a data point from one of five independent experiments. *D*, representative FLAG Western blot (*WB*) showing CBGC-3xFLAG-Gβ_5 and 3xFLAG-R7BP expression for each condition in *C*. The band marked with an *asterisk* is a degradation product of CBGC-3xFLAG-Gβ_5. *E*, Gα_{13}(Q/L)-CBGN-EE expression does not change with co-expression of R7-RGS heterotrimer proteins. Shown are representative immunoblots for *C*. *Error bars* indicate standard deviation of the mean. Statistical significance was determined using two-tailed, two-sample Student's *t* test assuming equal or unequal variance as deemed appropriate by F-test analysis. *, $p < 0.05$; **, $p < 0.01$; ***, $p < 0.001$; *n.s.*, $p > 0.05$.

presence of R7BP (Fig. 3*B*), presumably because palmitoylated R7BP targets R7-RGS·Gβ_5 complexes to the plasma membrane where Gα_{13} localizes.

Next we used split-luciferase complementation to determine whether complexes containing any R7-RGS isoform can interact with Gα_{13} or whether particular R7-RGS family members are preferred. For these experiments, HEK293 cells were transfected with Gα_{13}(Q/L)-CBGN and CBGC-FLAG-Gβ_5 with various R7-RGS isoforms in the presence or absence of R7BP. Because the proteolytic stability of Gβ_5 varies depending on which R7-RGS isoform is expressed in the presence or absence of R7BP and because luciferase signals depend on the expression level of CBGC-FLAG-Gβ_5, we normalized split-luciferase signals in these experiments to the expression of CBGC-FLAG-Gβ_5 determined by immunoblotting (Fig. 3*D*). Normalization for Gα_{13}(Q/L)-CBGN expression was unnecessary because this protein was well expressed with or without RGS7 or R7BP as indicated by immunoblotting of glutamate-glutamate (EE)-

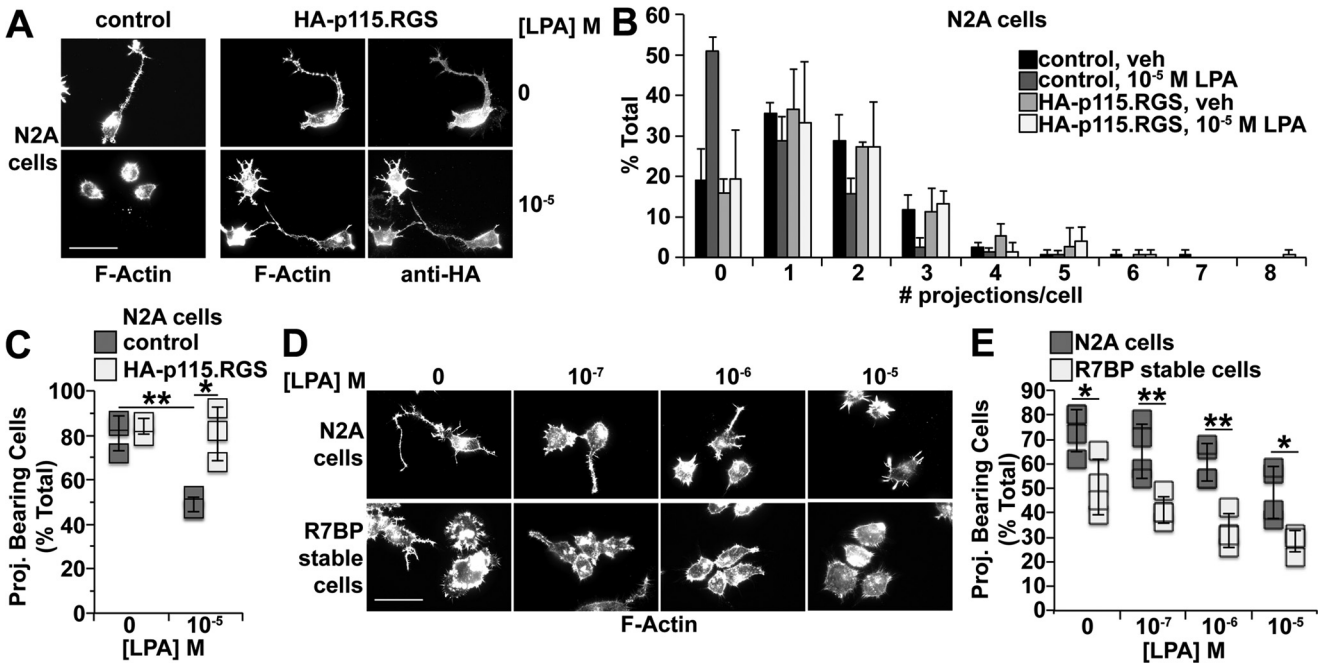

Figure 4. R7BP augments neurite retraction evoked by activation of $G\alpha_{12/13}$-coupled LPA receptors or serum starvation. Rhodamine-phalloidin staining and fluorescence microscopy were used to visualize neurites and cell morphology. Cells were scored by counting the number of neurites elaborated from the cell body that were greater than half the cell body diameter. At least 50 cells were scored per condition per experiment. *A*, representative fluorescence images of parental N2a cells transfected with either GFP (control) or HA-p115·RGS and treated with vehicle (*veh*) or 10 μM LPA. Control experiments confirmed antibody staining specificity (data not shown). *B*, quantification of neurites formed per cell under conditions shown in *A*. Data shown are the average of three independent experiments. *C*, number of cells with neurites under conditions shown in *A*. Each *box* represents a data point from one of three independent experiments. *D*, representative fluorescence images of parental N2a or N2a cells stably expressing FLAG-R7BP treated with the indicated concentrations of LPA. *E*, quantification of neurite formation under conditions shown in *D*. Each *box* represents a data point from one of four independent experiments. *Scale bars*, 50 μm. *Error bars* indicate standard deviation of the mean. Statistical significance was determined using two-tailed, two-sample Student's *t* test assuming equal or unequal variance as deemed appropriate by F-test analysis. *, $p < 0.05$; **, $p < 0.01$. *Proj.*, projection.

tagged $G\alpha_{13}$(Q/L)-CBGN (Fig. 3*E*). Data analyzed in this way showed efficient luciferase complementation when $G\alpha_{13}$(Q/L)-CBGN was co-expressed with CBGC-FLAG-$G\beta_5$, R7BP, and any R7-RGS family member, whereas complementation was low in the absence of either an R7-RGS subunit or R7BP (Fig. 3*C*). Therefore, $G\alpha_{13}$ interacted in living cells with heterotrimers bearing R7BP, $G\beta_5$, and any R7-RGS isoform.

R7-RGS heterotrimers augment neurite retraction evoked by $G\alpha_{13}$-coupled lysophosphatidic acid (LPA) receptors

To determine whether R7-RGS heterotrimers affect biological processes driven by $G\alpha_{13}$ and its close paralog $G\alpha_{12}$, we took advantage of studies showing that $G\alpha_{12/13}$ signaling causes growth cone collapse and neurite retraction in cultured neurons and neuronal cell lines (38–44). Accordingly, we determined whether R7-RGS heterotrimers affect neurite retraction in differentiated N2a cells. N2a cells were chosen as a model because they elaborate neurites when differentiated by serum starvation, and expression of constitutively active $G\alpha_{13}$ or RhoA in these cells antagonizes neurite elaboration (40, 44). Moreover, N2a cells endogenously express RGS7 and $G\beta_5$ but lack R7BP (5), which allowed us to compare $G\alpha_{12/13}$-driven processes in the absence or presence of R7BP stably transfected at physiological levels to promote interaction of R7-RGS complexes with $G\alpha_{13}$.

LPA evokes neurite retraction in primary neurons by activating receptors coupled to $G\alpha_{12/13}$ (41, 42). Whether LPA triggers neurite retraction in N2a cells had not been established, although this seemed likely because expression of constitutively active $G\alpha_{13}$ in these cells antagonizes neurite formation. To address this question, we differentiated N2a cells by serum starvation and treated them with LPA for 15 min. After fixation and permeabilization, cells were stained with rhodamine-phalloidin to visualize neurites and actin organization. We found that LPA treatment robustly evoked neurite retraction (Fig. 4, *A–C*). Because LPA receptors can couple to $G_{i/o}$, $G_{q/11}$, G_s, and $G_{12/13}$ (45), we determined whether LPA-induced neurite retraction in differentiated N2a cells is mediated by $G_{12/13}$ signaling. To address this question, we inhibited $G_{12/13}$ signaling by overexpressing a truncated HA-tagged version of p115-RhoGEF (HA-p115·RGS) that is targeted to the plasma membrane by a prenylation motif and retains GAP activity for $G\alpha_{12/13}$ but cannot activate RhoA (46). Expression of HA-p115·RGS blocked LPA-induced neurite retraction in differentiated N2a cells (Fig. 4, *A–C*), indicating that $G_{12/13}$ signaling is indeed required for this process.

Based on the preceding results, we investigated whether R7-RGS heterotrimers can regulate LPA-induced neurite retraction. Because R7BP facilitates interaction between R7-RGS complexes and $G\alpha_{13}$, we compared the effects of LPA on N2a cells, which express RGS7 and $G\beta_5$ but lack R7BP (5), with N2a cells stably expressing FLAG-R7BP at physiological levels (5). Results indicated that LPA-evoked neurite retraction was augmented in cells expressing FLAG-R7BP (Fig. 4, *D* and *E*), suggesting that R7BP-bound R7-RGS complexes augment signaling by $G_{12/13}$-coupled LPA receptors.

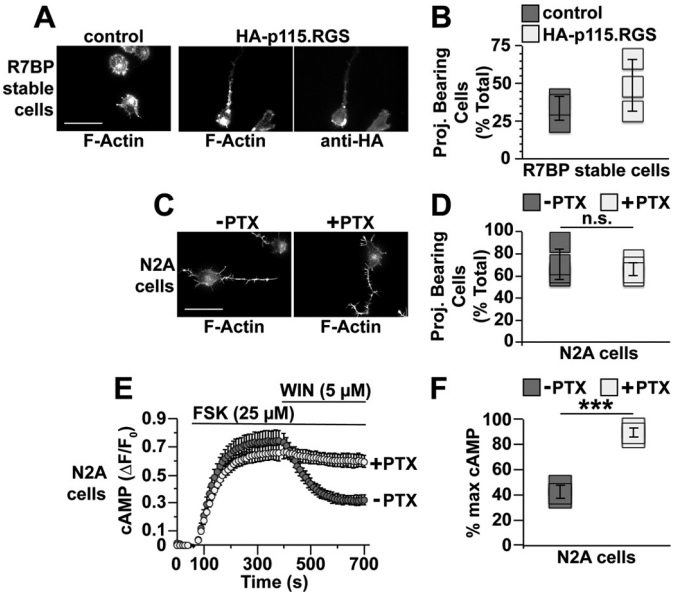

Figure 5. $G\alpha_{12/13}$ activity rather than $G\alpha_{i/o}$ activity regulates neurite formation by serum-starved N2a cells. N2a cells lacking or stably expressing 3xFLAG-R7BP were plated, differentiated, fixed, stained, and scored as described in Fig. 4 and under "Experimental procedures." *A*, representative fluorescence images of cells stably expressing FLAG-R7BP and transfected with either GFP (control) or HA-p115·RGS. *B*, quantification of neurite formation under conditions shown in *A*. In these experiments, all cells quantified were transfected, whereas those in Fig. 4*E* were not transfected, which likely explains why the percentage of R7BP-expressing cells bearing neurites in response to serum starvation was different between the two types of experiments. Each *box* represents a data point from one of three independent experiments. *C*, representative fluorescence images of parental N2a cells treated with PTX. *D*, quantification of the neurites formed by cells under conditions described in *C*. Each *box* represents a data point from one of four independent experiments. *E*, inhibition of $G_{i/o}$ signaling by PTX in N2a cells. N2a cells were transfected with the cAMP FRET sensor Epac-S^{H187} and treated for 16–24 h with or without 100 ng/ml PTX. Baseline cAMP levels were recorded for 1 min, and then cells were treated with 25 μM forskolin (*FSK*) to stimulate cAMP production. After 5 min of forskolin treatment, endogenous $G_{i/o}$-coupled cannabinoid type 1 receptors were activated by addition of 5 μM WIN 55,212-2 (*WIN*), and cAMP levels were recorded for an additional 5 min. Data shown are the averages of three independent experiments. *F*, quantification of percent maximum cAMP levels after WIN 55,212-2 stimulation as shown in *E*. Percent maximum (% *max*) cAMP = [(minimum $\Delta F/F_0$)/(maximum $\Delta F/F_0$)] × 100. Each *box* represents a data point from one of three independent experiments. *Scale bars*, 50 μm. *Error bars* indicate standard deviation of the mean. Statistical significance was determined using two-tailed, two-sample Student's *t* test assuming equal variance as deemed appropriate by F-test analysis. ***, $p < 0.001$; *n.s.*, $p > 0.05$. *Proj.*, projection.

In the preceding experiments, we also noted that, prior to LPA stimulation, R7BP expression antagonized neurite formation evoked by serum starvation alone (Fig. 4, *D* and *E*). To explore the mechanisms involved, we tested two models. In the first model, R7BP expression enables R7-RGS complexes to augment serum starvation-evoked $G_{12/13}$ signaling, which attenuates neurite formation. If so, inhibiting $G_{12/13}$ activity would be expected to rescue neurite formation in N2a cells stably expressing FLAG-R7BP. To test this prediction, FLAG-R7BP-expressing N2a cells were transiently transfected with HA-p115·RGS or a GFP-expressing control plasmid, differentiated, and analyzed for neurite formation. Results indicated that neurite formation trended higher but was incompletely rescued in cells transiently expressing HA-p115·RGS as compared with controls (Fig. 5, *A* and *B*; $p = 0.24$). Thus, R7BP-bound R7-RGS heterotrimers appeared to regulate neurite morphogenesis under basal conditions in serum-starved cells by mechanisms that depend partly on $G_{12/13}$ signaling.

One potential explanation for the preceding result is provided by a second model in which R7BP-bound R7-RGS complexes regulate neurite morphogenesis in serum-starved cells in part by attenuating $G_{i/o}$ signaling. Indeed, $G_{i/o}$-coupled cannabinoid type 1 receptor signaling promotes neurite outgrowth in N2a cells (47, 48), which potentially could be negatively regulated by the GAP activity of R7BP-bound R7-RGS complexes (17, 23, 49–51). However, whether $G_{i/o}$ activity in N2a cells promotes neurite formation in response to serum starvation had not been tested. We found that this appeared not to be the case because blocking $G_{i/o}$ activation with pertussis toxin (PTX) did not inhibit neurite formation evoked by serum starvation (Fig. 5, *C* and *D*) in contrast to control experiments demonstrating that PTX treatment strongly inhibited the ability of a cannabinoid type 1 agonist (WIN 55,212-2) to blunt forskolin-evoked cAMP accumulation detected with a FRET reporter (Fig. 5, *E* and *F*). Therefore, these results argued against models in which R7BP-bound R7-RGS complexes promote neurite retraction by attenuating $G_{i/o}$ signaling.

Lastly, we explored how R7BP augments $G\alpha_{13}$-dependent neurite retraction by studying $G\alpha_{13}$-activated RhoGEFs (LARG, p115RhoGEF, and PDZ-RhoGEF) that mediate RhoA activation and consequent neurite retraction. Our initial approach relied on prior investigations showing that these RhoGEFs can be recruited to the plasma membrane by activated $G\alpha_{13}$ (46). Thus, if R7BP-bound R7-RGS complexes promote $G\alpha_{13}$ signaling, then expression of R7BP in N2a cells might be expected to augment plasma membrane recruitment of these RhoGEFs. However, by confocal imaging, we were unable to detect differences in plasma membrane recruitment of GFP-tagged LARG, p115RhoGEF, or PDZ-RhoGEF in response to LPA and/or R7BP expression (data not shown).

As an alternative approach that might provide greater sensitivity, we determined whether RhoGEFs affect interaction between constitutively active $G\alpha_{13}$ and R7BP-bound R7-RGS complexes in split-luciferase complementation assays. Rather than assessing $G\alpha_{13}$ activity, this approach addressed the key question whether complexes containing activated $G\alpha_{13}$ and R7-RGS heterotrimers are capable of physically engaging effector RhoGEFs that trigger RhoA activation and neurite retraction. Accordingly, HEK293 cells were transfected with $G\alpha_{13}$(Q/L)-CBGN, CBGC-FLAG-Gβ_5, RGS7, and R7BP in the absence or presence of Myc-tagged forms of LARG, p115RhoGEF, or PDZ-RhoGEF. As shown in Fig. 6, split-luciferase complementation resulting from interaction between activated $G\alpha_{13}$ and R7BP-bound RGS7-Gβ_5 complexes was increased ~7-fold by LARG, 4-fold by PDZ-RhoGEF, and 2-fold by p115RhoGEF. Accordingly, the results of these and preceding experiments support models in which R7BP-bound R7-RGS complexes interact with $G\alpha_{13}$ in neuronal cells to augment signaling mechanisms that promote neurite retraction and blunt neurite formation.

Discussion

Our findings are the first to indicate that R7-RGS heterotrimers form macromolecular complexes with $G\alpha_{13}$ and con-

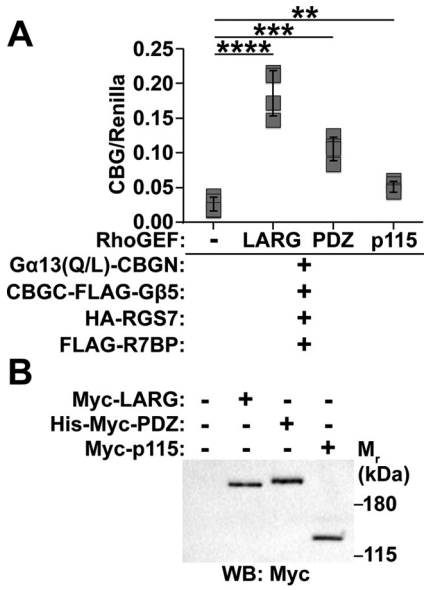

Figure 6. RH-RhoGEFs enhance interaction between $G\alpha_{13}$ and R7-RGS heterotrimers. *A*, split-luciferase complementation between $G\alpha_{13}$(Q/L)-CBGN and CBGC-FLAG-$G\beta_5$ co-expressed with HA-RGS7 and FLAG-R7BP with or without Myc-LARG, His-Myc-PDZ-RhoGEF, or Myc-p115RhoGEF. Each *box* represents a data point from one of four independent experiments. *B*, representative Myc Western blot (*WB*) showing Myc-LARG, His-Myc-PDZ-RhoGEF, and Myc-p115RhoGEF protein expression levels for conditions used in *A*. *Error bars* indicate standard deviation of the mean. Statistical significance was determined using two-tailed, two-sample Student's *t* test assuming equal variance as deemed appropriate by F-test analysis. **, $p < 0.01$; ***, $p < 0.001$; ****, $p < 0.0001$.

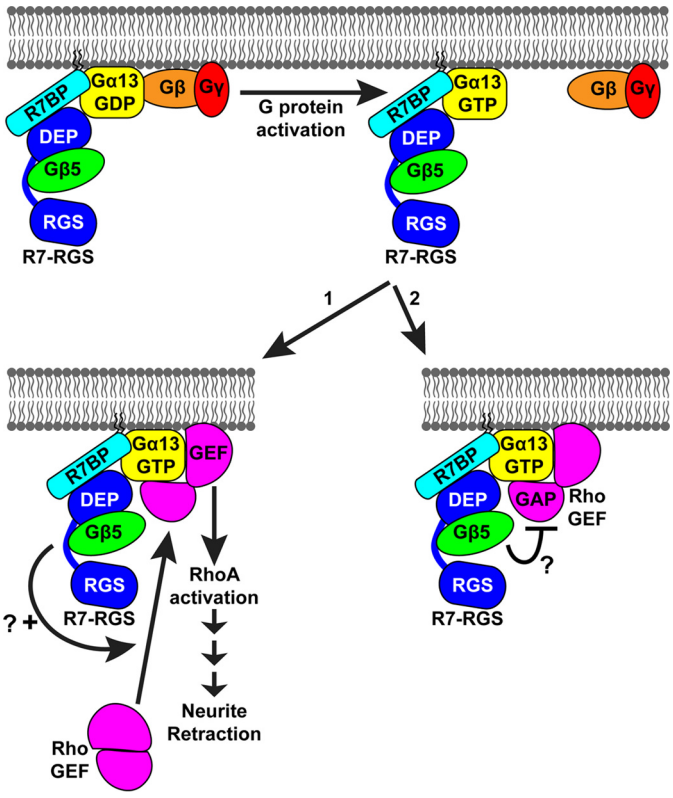

Figure 7. Models for enhancement of $G\alpha_{13}$-evoked neurite retraction by R7-RGS heterotrimers. R7-RGS heterotrimers form macromolecular complexes with G_{13} heterotrimers and remain bound to $G\alpha_{13}$ upon activation of the G protein. Activated $G\alpha_{13}$ recruits a RhoGEF to the plasma membrane where it activates RhoA and downstream signaling events that ultimately result in neurite retraction. RhoGEFs also negatively regulate this process because they are GAPs for $G\alpha_{13}$. R7-RGS heterotrimers could facilitate $G\alpha_{13}$-evoked neurite retraction by two non-mutually exclusive mechanisms: *1*) enhancing recruitment and activation of RhoGEFs, thereby enhancing RhoA signaling, or *2*) inhibiting RhoGEF GAP activity for $G\alpha_{13}$, thereby prolonging $G\alpha_{13}$ activity.

trol neurite morphogenesis regulated in part by $G_{12/13}$-dependent signaling. Accordingly, they expand the functional diversity of R7-RGS heterotrimers beyond their canonical roles as GAPs for $G\alpha_{i/o}$. Because genetic ablation of R7-RGS complexes affects diverse aspects of neurological development and function (9–12), our findings suggest that R7-RGS heterotrimers potentially regulate certain processes in part by augmenting $G\alpha_{13}$ signaling rather than solely by attenuating $G_{i/o}$ signaling. Indeed, certain phenotypes of mice lacking R7-RGS heterotrimers are not recapitulated in mice expressing RGS-insensitive mutant forms of $G\alpha_o$ or $G\alpha_i$ (52).

Several prior lines of evidence are consistent with the hypothesis that R7-RGS heterotrimers regulate $G_{12/13}$ signaling to control nervous system development. R7-RGS heterotrimers are dramatically up-regulated during postnatal brain development as synapses mature (5, 53). Mice lacking all R7-RGS complexes exhibit abnormal Purkinje cell maturation and dendritic arborization, delayed morphological development of the hippocampus, and increased ectopic granule cells in the hippocampus (10). These postnatal neurological phenotypes potentially could be caused in part by diminished $G_{12/13}$ signaling, which controls similar processes during embryonic brain development. For example, conditional ablation of $G\alpha_{13}$ and its paralog $G\alpha_{12}$ in the nervous system causes overmigration of cortical plate and Purkinje neurons in embryonic mice (41). Accordingly, increased ectopic granule cells in the hippocampus of mice lacking all R7-RGS complexes might arise from overmigration of these cells because $G\alpha_{13}$ activity is reduced and fails to provide sufficiently strong migratory "stop" signals, similar to what occurs for cortical plate neurons and cerebellar Purkinje cells in embryonic $G\alpha_{13}{}^{-/-}$ mice. Further evidence linking $G\alpha_{13}$ and R7-RGS complexes is provided by the observation that $G\alpha_{13}$ mRNA is up-regulated in cerebellum of 2-week-old postnatal mice lacking all R7-RGS complexes (11) potentially to compensate for diminished $G\alpha_{13}$ signaling activity caused by the absence of R7-RGS complexes.

Establishing the biological functions of $G\alpha_{13}$ signaling regulated by R7-RGS heterotrimers will require understanding the molecular mechanisms involved. Although much remains to be learned, we suggest two mechanistic hypotheses (Fig. 7), which are not mutually exclusive; other models also can be imagined. Both models are consistent with our findings that R7-RGS heterotrimers can interact with $G\alpha_{13}$ regardless of its activity state and that this interaction is augmented by $G\alpha_{13}$-regulated RhoGEFs. In the first model, R7BP-bound R7-RGS heterotrimers interact with $G\alpha_{13}$ to facilitate RhoGEF signaling that promotes neurite retraction (46). Consistent with this mechanism, targeting p115RhoGEF to the plasma membrane by appending a prenylation motif triggers neurite retraction in PC12 cells (46), which express R7BP and R7-RGS complexes (55). In a second model, R7-RGS heterotrimers are proposed to augment neurite retraction by inhibiting deactivation of $G\alpha_{13}$ via the GAP activity of RGS domain-containing RhoGEFs. This model is sug-

gested by evidence that certain RGS domains possess allosteric inhibitory sites distal to the surface that binds Gα subunits to stimulate GTP hydrolysis (56, 57). Whether such inhibitory sites exist in the RGS domains of $G\alpha_{12/13}$-activated RhoGEFs and are targeted by R7-RGS complexes remains to be investigated. Distinguishing between these two models would require determining whether R7BP-bound R7-RGS complexes regulate the activation or deactivation of $G\alpha_{13}$ and RhoGEFs *in vitro*.

Whether $G_{12/13}$ signaling is facilitated similarly by complexes containing any R7-RGS isoform is unclear. Although we found that $G\alpha_{13}$ can interact with heterotrimers containing any R7-RGS subtype, our functional studies were limited to N2a cells in which RGS7 appears to be the principal R7-RGS isoform expressed.[3] Indeed, biological processes mediated by distinct G protein subtypes can be regulated by distinct R7-RGS isoforms as indicated by studies of the R7-RGS proteins Egl-10 and Eat-16 in *C. elegans* (25). Thus, it would be important to determine whether $G_{12/13}$ signaling also can be augmented by R7-RGS heterotrimers bearing RGS6, -9, or -11.

R7-RGS heterotrimers also may control neurite morphogenesis by regulating signaling mechanisms independent of $G\alpha_{13}$. This hypothesis is suggested by our finding that the neurite morphogenesis deficit of serum-starved R7BP-expressing N2a cells was rescued incompletely by expression of the $G_{12/13}$ inhibitor HA-p115·RGS. In contrast, LPA-evoked neurite retraction absolutely required $G_{12/13}$ signaling as indicated by complete blockade of this process by HA-p115·RGS. Further studies will be required to determine precisely how R7-RGS heterotrimers regulate neurite morphogenesis by $G\alpha_{13}$-dependent and -independent mechanisms.

In conclusion, we have identified a novel interaction between R7-RGS heterotrimers and $G\alpha_{13}$ and provided evidence that R7-RGS heterotrimers augment the function of $G\alpha_{13}$ as a regulator of neurite morphogenesis. Our findings expand understanding of R7-RGS heterotrimers as multifunctional complexes critical for diverse aspects of neuronal development and function.

Experimental procedures

Reagents and antibodies

The following commercially produced antibodies were used: mouse anti-GAPDH (GeneTex, catalog number GTX627408, lot 40953), mouse anti-FLAG M2 (Sigma, catalog number F1804, various lots), mouse anti-actin C4 (Millipore, catalog number MAB1501, lot NG1812617), mouse anti-EE (Covance, catalog number MMS-115P, lot E12BF00285), mouse anti-HA.11 (Covance, catalog number MMS-101R), mouse anti-Myc 9E10 (Covance, catalog number MMS-150R, lot 139023001), HRP-conjugated goat anti-mouse IgG (Thermo Scientific, catalog number 31430, various lots), HRP-conjugated goat anti-rabbit IgG (Thermo Scientific, catalog number 31460, various lots), and Alexa Fluor 488-conjugated goat anti-mouse IgG (Invitrogen, catalog number A11001, lot 481679). Our rabbit anti-R7BP polyclonal antibody has been described (5). Rabbit anti-$G\beta_5$ (ATDG) and rabbit anti-RGS7 (R4613) antibodies were generous gifts from Drs. William Simonds and Theodore Wensel, respectively (58, 59). Other reagents were as follows: Complete protease inhibitor mixture tablets (Roche Applied Science, catalog number 11697498001), mouse anti-FLAG M2-agarose (Sigma, catalog number A-2220), DSS (Thermo Scientific, catalog number 21555), StrepTactin Superflow (IBA, catalog number 2-1206-002), D-desthiobiotin solution (IBA, catalog number 2-1000-025), 3xFLAG peptide (Sigma, catalog number F4799), SYPRO Ruby stain (Sigma, catalog number S4942), Dual-Luciferase Reporter Assay System (Promega, catalog number E1960), LPA (Avanti Polar Lipids, catalog number 857130P), rhodamine-conjugated phalloidin (Life Technologies, catalog number R415), poly-D-lysine (Sigma, catalog number P0899), pertussis toxin (Calbiochem, catalog number 516561), forskolin (Sigma, catalog number F6886), and WIN 55,212-2 (Sigma, catalog number W102). All remaining reagents were from Sigma unless noted otherwise.

Generation of SF-R7BP transgenic mice

All procedures involving mice were conducted under protocols approved by the Animal Studies Committee of Washington University School of Medicine. To generate mice expressing SF-R7BP in neurons, a vector was generated to target SF-R7BP under control of the mouse prion promoter to the *Hprt* locus on the X chromosome. The backbone of the targeting vector was a modified version of pHPRT-targeting-Tet-EGFP-protein-entry (generously provided by Dr. Andrey Shaw) in which everything between the HPRT-targeting arms (including the Tet promoter and GFP) was replaced with a multiple cloning site and a PGK-Neo cassette. A transgene consisting of the mouse prion protein (MoPRP) promoter, MoPRP 5′-intronic sequence, SF-R7BP, and MoPRP 3′-untranslated region was inserted in reverse orientation in the multiple cloning site of the parent targeting vector. The MoPRP sequences were originally from the MoPrP·XhoI plasmid (34), and the SF tag sequence was originally from N-SF-TAP-pcDNA3 (a gift from Dr. Christian Johannes Gloeckner; Ref. 60). Standard methods were used to transfect ES cells with the targeting construct by electroporation (Washington University Murine Embryonic Stem Cell Core). Homologous recombination of the transgene causes deletion of exon 1 of *Hprt*, resulting in loss of HPRT protein expression and resistance to 6-thioguanine. Homologous recombinants were selected using both G418 and 6-thioguanine. ES cells that survived the selection process were confirmed as homologous recombinants by PCR using a forward primer specific for the PGK-Neo cassette on the transgene and a reverse primer specific for an HPRT genomic sequence outside of the right targeting arm. ES cells that were positive in the PCR test and had a normal karyotype were used for injection into C57BL/6 mouse blastocysts (Washington University School of Medicine, Department of Pathology Microinjection Core Facility) to generate chimeric mice. Chimeric male mice were bred with female C57BL/6 mice (Charles River) to produce offspring that were screened for germ line transmission by PCR. Mice positive for the SF-R7BP transgene were crossbred with $R7BP^{-/-}$ mice (50) to generate $R7BP^{+/-}$ offspring that

[3] S. L. Scherer, M. D. Cain, S. M. Kanai, K. M. Kaltenbronn, and K. J. Blumer, unpublished data.

also contained the SF-R7BP transgene. These offspring were subsequently crossed to generate $R7BP^{-/-}$ mice that were positive for the SF-R7BP transgene. Because endogenous R7BP is not expected to affect the makeup of the protein interaction profile, SF-R7BP male mice with both $R7BP^{+/-}$ and $R7BP^{-/-}$ backgrounds were used for TAP experiments based on availability.

Cell culture and transfection

All cells were maintained in DMEM/F-12 (Gibco, catalog number 11330-032) supplemented with 10% (v/v) FBS (Atlanta Biologicals, catalog number S11150) and penicillin/streptomycin at 37 °C with 5% CO_2 in a humidified incubator. Growth medium for 3xFLAG-R7BP stable cells also contained 200 μg/ml Geneticin (Gibco, catalog number 10131). Chemical cross-linking experiments used a previously described clonal derivative of N2a cells stably expressing 3xFLAG-R7BP (5). Microscopy experiments used N2a cells transfected with 3xFLAG-R7BP (17) and treated with 400 μg/ml Geneticin for 16 days to select cells that stably express 3xFLAG-R7BP. Transfections were performed using TransIT-LT1 transfection reagent (Mirus, catalog number MIR 2305) according to the manufacturer's protocol.

Plasmids

pcDNA3.1+ was the backbone for all constructs unless stated otherwise. CBGN-Gα fusion sequences were made using overlap extension PCR to insert a glycine/serine linker (GGGSSGGG) followed by CBGN and another glycine/serine linker (GGGSSGGG) into $G\alpha_{13}$ and $G\alpha_q$ between residues 135 and 136 and between residues 124 and 125, respectively. Split-luciferase fragments were amplified from plasmids containing fragments of click beetle green 99 luciferase (CBGN, amino acids 2–412; CBGC, amino acids 396–542; generous gifts from Dr. David Piwnica-Worms; Ref. 36). Human $G\alpha_{13}$ and $G\alpha_q$ were amplified from plasmids purchased from Missouri University of Science and Technology cDNA Resource Center. Constitutively active point mutants (Q226L) of $G\alpha_{13}$-CBGN and $G\alpha_q$-CBGN were generated using site-directed mutagenesis. $G\alpha_{13}$-CBGN-EE was generated using overlap extension PCR to mutate $G\alpha_{13}$ amino acids 188–193 from DYIPSQ to EYMPTE. CBGC-LARG·RGS was created using overlap extension PCR to splice CBGC followed by a glycine/serine linker and BglII restriction site to sequences encoding the RGS domain of human LARG (amino acids 348–558). CBGC-RGS2 was constructed by splicing CBGC followed by a glycine/serine linker and 3xFLAG sequence to sequences encoding the N terminus of human RGS2. CBGC-3xFLAG-$G\beta_5$ was generated by first constructing a plasmid containing CBGC followed by a glycine/serine linker and a 3xFLAG sequence immediately upstream of the multiple cloning site of pcDNA3.1+. The coding sequence of the short isoform of human $G\beta_5$ ($G\beta_5$s) was inserted in-frame into this plasmid. A plasmid that expresses plasma membrane-localized HA-p115·RGS was constructed by using overlap extension PCR to fuse sequences encoding a glycine/serine linker followed by the last 20 amino acids of human H-Ras to the C terminus of HA-p115·RGS (amino acids 1–252 of human p115RhoGEF). The plasmid expressing 3xFLAG-R7BP has been described (17). All newly described constructs were verified by DNA sequencing. Published plasmids expressing *Renilla* luciferase and HA-tagged R7-RGS proteins were generous gifts from Drs. David Piwnica-Worms and T. Kendall Harden, respectively. Plasmids expressing Myc-LARG, His-Myc-PDZ-RhoGEF, and Myc-p115RhoGEF were generous gifts from Dr. Tohru Kozasa. The plasmid expressing Epac-S^{H187} cAMP FRET sensor was generously provided by Dr. Kees Jalink (61).

In-cell chemical cross-linking

Wild-type N2 cells or N2a cells stably expressing 3xFLAG-R7BP were trypsinized, pelleted, and washed twice with PBS. Cross-linking reagents were prepared just before use by making a 200 mM stock of DSS in DMSO and then diluting in 100 mM HEPES (pH 8) for a final working solution of 1 mM DSS in 5% (v/v) DMSO. Cells were suspended in 1 mM DSS solution at 2.2×10^6 cells/ml and incubated for 30 min at room temperature. Cross-linking reactions were quenched by adding 20 mM Tris (pH 7.4) and incubating for 15 min at room temperature. Cells were then pelleted and lysed for immunoprecipitation.

Immunoblotting and immunoprecipitation

The following immunoprecipitation protocol was used for the data shown in Fig. 1*A*. Cells were lysed in radioimmune precipitation assay buffer (150 mM NaCl, 10 mM sodium phosphate, 1% (w/v) sodium deoxycholate, 1% (v/v) IGEPAL CA-630, 0.5% (w/v) SDS, 1 mM DTT, Complete protease inhibitor mixture) by agitating for 30 min at 4 °C and then cleared by ultracentrifugation at 100,000 $\times$ *g* for 10 min at 4 °C. Cross-linked species containing 3xFLAG-R7BP were immunoprecipitated by incubating with mouse anti-FLAG M2-agarose for 2 h at 4 °C followed by three washes with radioimmune precipitation assay buffer and eluted by boiling with 2× SDS-PAGE sample buffer (50 mM Tris (pH 6.8), 2% (w/v) SDS, 10% (v/v) glycerol, 1% (v/v) 2-mercaptoethanol, 12.5 mM EDTA, 0.02% (w/v) bromphenol blue) for 10 min.

Tissue lysates for experiments shown in Fig. 1*C* were generated by the following protocol. Mice were euthanized by asphyxiation with CO_2 followed by cervical dislocation. The indicated tissues were isolated, and brains were further dissected in Hanks' balanced salt solution (Gibco, catalog number 14175) followed by homogenization in TAP lysis buffer (30 mM Tris (pH 7.4), 150 mM NaCl, 0.5% (v/v) IGEPAL CA-630, 0.5% (w/v) deoxycholate, Complete protease inhibitor mixture) using a Dounce homogenizer and then transferred to tubes and rotated end-over-end for 30 min at 4 °C. Lysates were cleared by ultracentrifugation at 100,000 $\times$ *g* for 15 min at 4 °C. A Bradford assay was performed to determine total protein content in the cleared lysates to equalize protein loading for SDS-PAGE.

All Western blot analyses were performed according to the following protocol. Samples were separated by SDS-PAGE, transferred to PVDF (Millipore, catalog number IPVH00010), blocked for at least 1 h using 5% (w/v) milk in TBST (25 mM Tris (pH 7.2), 150 mM NaCl, 2.7 mM KCl, 0.1% (v/v) Tween 20), incubated with the indicated primary antibody in blocking

buffer for at least 2 h, washed three times with TBST, incubated for 1 h with appropriate HRP-conjugated secondary antibodies diluted in blocking buffer, and washed three times with TBST. Signals were detected using ECL solution (GE Healthcare, catalog number RPN2106, or Bio-Rad, catalog number 170-5060) and either film or a ChemiDoc Imaging System (Bio-Rad). In some cases after image acquisition, membranes were rinsed, reblocked, and probed for another protein. All quantified Western blot signals were within the linear range of the detection system as determined by an independent standard curve.

Tandem affinity purification

TAP was performed as described previously with following modifications (32). Three adult male mice expressing SF-R7BP (one $R7BP^{-/-}$ and two $R7BP^{+/-}$) were euthanized by asphyxiation with CO_2 followed by cervical dislocation. All subsequent steps were performed on ice or at 4 °C. Whole brains were dissected, homogenized with a Dounce homogenizer in lysis buffer (30 mM Tris (pH 7.4), 150 mM NaCl, 0.5% (v/v) IGEPAL CA-630, 0.5% (w/v) deoxycholate, Complete protease inhibitor mixture), rotated end-over-end for 30 min, cleared by ultracentrifugation at 100,000 × *g* for 15 min, and cleared further by passing through a 0.22-μm polyethersulfone filter. Cleared lysates were incubated with StrepTactin resin overnight with end-over-end rotation and washed five times in batch with a 10× column volume of wash buffer (30 mM Tris (pH 7.4), 150 mM NaCl, 0.1% (v/v) IGEPAL CA-630, Complete protease inhibitor mixture). Protein complexes were eluted two consecutive times by incubating with 3× column volumes of elution buffer (1× desthiobiotin buffer E (IBA), 0.1% (v/v) IGEPAL CA-630, Complete protease inhibitor mixture) for 30 min in batch. StrepTactin elution fractions were combined and incubated with anti-FLAG M2-agarose in batch for 1 h and washed five times in batch with 10× column volumes of wash buffer. Protein complexes were eluted from FLAG-agarose by incubating with 4× column volumes of FLAG elution buffer (200 μg/ml 3xFLAG peptide in wash buffer) for 30 min in batch. The final eluate was concentrated in preparation for gel electrophoresis using an Amicon Ultra-0.5 10,000 centrifugal filter device (Millipore, catalog number UFC501008).

LC-MS/MS

Mass spectrometry analysis was performed by the Proteomics and Mass Spectrometry Facility at the Donald Danforth Plant Science Center (St. Louis, MO). The final TAP eluate described above was resolved by SDS-PAGE, and protein bands were visualized with SYPRO Ruby (Fig. 2*C*). Prominent bands were excised, and proteins were digested using trypsin and Glu-C and analyzed by LC-MS/MS using a 1-h gradient and an LTQ-Orbitrap mass spectrometer. Peak lists were generated using Mascot Distiller version 2.4. Mass spectrometric data were searched using Mascot version 2.4.1 search engine and NCBInr Mammalia database (April 2013 version; 1,392,029 entries). The following parameters were used: trypsin and Glu-C allowed proteases, two missed cleavages allowed, no fixed modifications allowed, +16 on Met (oxidation) allowed as a variable modification, 15-ppm mass tolerance for precursor ions, and 0.80-Da mass tolerance for fragment ions. The database cRAP_20110301 (118 entries) was used to exclude known contaminants. Scaffold (version 4.0.5) was used to validate peptide and protein identities. Peptide identifications were accepted if they could be established at greater than 80% probability by the Scaffold local false discovery rate algorithm. All reported proteins have at least 99% protein identification probabilities as determined using the Protein Prophet algorithm and at least two exclusive unique peptides assigned. Proteins that contained similar peptides and could not be differentiated based on MS/MS analysis alone were grouped to satisfy the principles of parsimony. Proteins sharing significant peptide evidence were grouped into clusters. Glu-C, trypsin, and keratin proteins were removed manually from the results. Reported are the proteins identified from a single TAP experiment starting with three SF-R7BP mouse brains.

Split-luciferase complementation

HEK293 cells were plated in 24-well dishes and transfected the next day with the indicated split-luciferase plasmids, *Renilla* luciferase for signal normalization, GFP to assess transfection efficiency, and pcDNA to normalize total DNA amounts across samples. At least three replicate wells of cells were transfected per condition in each independent experiment. Luciferase assays were performed 24–26 h after transfection using the Dual-Luciferase Reporter Assay System according to the manufacturer's protocol. A GloMax96 luminometer equipped with two injection pumps was used to measure luciferase activity on a per-well basis by first injecting the substrate solution for CBG and then injecting a quencher for click beetle green as well as the substrate for *Renilla* luciferase. Data collection started 0.4 s after substrate addition with a 10-s integration time.

Fluorescence microscopy

For microscopy experiments using HA-p115·RGS, cells were transfected and then replated the next day at low density on poly-D-lysine (PDL)-coated glass coverslips. For experiments not requiring transfection, cells were simply plated at low density on PDL-coated glass coverslips. Three hours after plating, the medium was exchanged for differentiation medium (DMEM/F-12 plus penicillin/streptomycin). For experiments using PTX, cells were plated at low density on PDL-coated glass coverslips and treated with 100 ng/ml PTX overnight. The next morning, the medium was exchanged for differentiation medium containing 100 ng/ml PTX, and this was repeated again 24 h later. In all cases, cells were allowed to differentiate for 48 h. If indicated, cells were treated with various concentrations of LPA (in 5 mg/ml fatty acid-free BSA in DPBS) for 15 min prior to fixing. Cells were fixed by incubation with 4% paraformaldehyde in DPBS (pH 7.2) for 10 min at room temperature followed by washes with DPBS. Fixed cells were permeabilized with 0.5% (v/v) Triton X-100 in DPBS for 10 min at room temperature, washed with DPBS, and blocked with blocking buffer (1% (w/v) BSA, 0.1% (v/v) Tween 20 in DPBS) for at least 30 min at room temperature. If immunostaining was required, coverslips were incubated with primary antibody (diluted in blocking buffer) in a humidified chamber overnight at 4 °C, washed three

times with wash buffer (0.1% (v/v) Tween 20 in DPBS), and incubated with appropriate Alexa Fluor-conjugated secondary antibody and rhodamine-conjugated phalloidin in a humidified chamber for 1 h at room temperature. For experiments that did not require immunostaining, rhodamine-phalloidin was incubated with the coverslips for 30 min in a humidified chamber at room temperature immediately following the permeabilization step. All coverslips were washed three times with wash buffer, rinsed briefly in water, and mounted on glass slides using Vectashield mounting medium. Microscopy images were acquired with an Olympus IX81 inverted fluorescence microscope equipped with a UPlanSApo 60× oil objective (numerical aperture, 1.35) and an EXi BLUE digital camera (Q Imaging). Images were acquired using MetaMorph for Olympus Advanced and processed using Fiji software. Brightness and contrast were adjusted on an entire-image basis. Images of rhodamine-phalloidin fluorescence were used to score neurite projections, defined as any process extending from the cell body that was longer than half the cell body length. Cell body lengths were measured using the line tool, and neurite lengths were measured using the segmented line tool in Fiji.

cAMP FRET sensor assay

N2a cells were transfected with the Epac-S^{H187} cAMP FRET sensor. After 24 h, cells were trypsinized and replated in a black-wall clear-bottom 96-well plate (Costar, catalog number 3603) coated with poly-D-lysine. Cells were incubated in serum-free medium with or without 100 ng/ml pertussis toxin for 16–24 h. Prior to imaging, growth medium was replaced with pre-warmed (37 °C) imaging buffer (125 mM NaCl, 5 mM KCl, 1.5 mM $MgCl_2$, 1.5 mM $CaCl_2$, 10 mM D-glucose, 20 mM HEPES (pH 7.4)) and assayed immediately using a Synergy H4 Hybrid Reader (BioTek) equipped with injection pumps for adding forskolin and WIN 55,212-2. Cells were maintained at 37 °C throughout the recording period. FRET donor was excited using a xenon flash lamp and a 420/20 bandpass filter. Donor emission and acceptor emission were detected every 10 s using 480/20 and 540/20 bandpass filters, respectively. A dichroic mirror with a 455-nm cutoff was used to separate the excitation and emission light paths. Changes in cAMP levels were expressed as follows.

$$\frac{\Delta F}{F_0} = \frac{\text{FRET ratio} - \text{baseline FRET ratio}}{\text{baseline FRET ratio}} \qquad \text{(Eq. 1)}$$

where FRET ratio = ($480\ nm^{emission}/540\ nm^{emission}$) at a given time point and the baseline FRET ratio = average ($480\ nm^{emission}/540\ nm^{emission}$) prior to forskolin stimulation. Triplicate wells were assayed per condition in each independent experiment.

Author contributions—S. L. S. designed and performed experiments, analyzed data, and wrote the paper. M. D. C. developed the split-luciferase system used in Figs. 3 and 6. K. M. K. designed, generated, and maintained SF-R7BP transgenic mice and performed experiments shown in Fig. 6. S. M. K. designed and performed experiments shown in Fig. 5, *E* and *F*. K. J. B. conceived and directed the study and wrote the paper. All authors approved the final version of the manuscript.

Acknowledgments—We thank Drs. Johannes Gloeckner, David Harris, David Piwnica-Worms, T. Kendall Harden, Andrey Shaw, Tohru Kozasa, Kees Jalink, and Philip Wedegaertner for providing plasmids; Drs. William Simonds and Theodore Wensel for providing antibodies; Drs. Leslie Hicks and Sophie Alvarez at the Danforth Center Proteomics facility for conducting proteomics experiments; and Joel Rurik for conducting confocal microscopy experiments.

References

1. Ross, E. M., and Wilkie, T. M. (2000) GTPase-activating proteins for heterotrimeric G proteins: regulators of G protein signaling (RGS) and RGS-like proteins. *Annu. Rev. Biochem.* **69,** 795–827
2. Hooks, S. B., Waldo, G. L., Corbitt, J., Bodor, E. T., Krumins, A. M., and Harden, T. K. (2003) RGS6, RGS7, RGS9, and RGS11 stimulate GTPase activity of G_i family G-proteins with differential selectivity and maximal activity. *J. Biol. Chem.* **278,** 10087–10093
3. Posner, B. A., Gilman, A. G., and Harris, B. A. (1999) Regulators of G protein signaling 6 and 7. Purification of complexes with $G\beta_5$ and assessment of their effects on G protein-mediated signaling pathways. *J. Biol. Chem.* **274,** 31087–31093
4. Snow, B. E., Krumins, A. M., Brothers, G. M., Lee, S.-F., Wall, M. A., Chung, S., Mangion, J., Arya, S., Gilman, A. G., and Siderovski, D. P. (1998) A G protein γ subunit-like domain shared between RGS11 and other RGS proteins specifies binding to Gβ5 subunits. *Proc. Natl. Acad. Sci. U.S.A.* **95,** 13307–13312
5. Grabowska, D., Jayaraman, M., Kaltenbronn, K. M., Sandiford, S. L., Wang, Q., Jenkins, S., Slepak, V. Z., Smith, Y., and Blumer, K. J. (2008) Postnatal induction and localization of R7BP, a membrane-anchoring protein for regulator of G protein signaling 7 family-Gβ5 complexes in brain. *Neuroscience* **151,** 969–982
6. Zhang, J. H., Lai, Z., and Simonds, W. F. (2000) Differential expression of the G protein β5 gene: analysis of mouse brain, peripheral tissues, and cultured cell lines. *J. Neurochem.* **75,** 393–403
7. Gold, S. J., Ni, Y. G., Dohlman, H. G., and Nestler, E. J. (1997) Regulators of G-protein signaling (RGS) proteins: region-specific expression of nine subtypes in rat brain. *J. Neurosci.* **17,** 8024–8037
8. Nishiguchi, K. M., Sandberg, M. A., Kooijman, A. C., Martemyanov, K. A., Pott, J. W., Hagstrom, S. A., Arshavsky, V. Y., Berson, E. L., and Dryja, T. P. (2004) Defects in RGS9 or its anchor protein R9AP in patients with slow photoreceptor deactivation. *Nature* **427,** 75–78
9. Krispel, C. M., Chen, C.-K., Simon, M. I., and Burns, M. E. (2003) Prolonged photoresponses and defective adaptation in rods of Gβ5−/− mice. *J. Neurosci.* **23,** 6965–6971
10. Rao, A., Dallman, R., Henderson, S., and Chen, C.-K. (2007) Gβ5 is required for normal light responses and morphology of retinal ON-bipolar cells. *J. Neurosci.* **27,** 14199–14204
11. Zhang, J.-H., Pandey, M., Seigneur, E. M., Panicker, L. M., Koo, L., Schwartz, O. M., Chen, W., Chen, C.-K., and Simonds, W. F. (2011) Knockout of G protein β5 impairs brain development and causes multiple neurologic abnormalities in mice. *J. Neurochem.* **119,** 544–554
12. Zachariou, V., Georgescu, D., Sanchez, N., Rahman, Z., DiLeone, R., Berton, O., Neve, R. L., Sim-Selley, L. J., Selley, D. E., Gold, S. J., and Nestler, E. J. (2003) Essential role for RGS9 in opiate action. *Proc. Natl. Acad. Sci. U.S.A.* **100,** 13656–13661
13. Siderovski, D. P., and Willard, F. S. (2005) The GAPs, GEFs, and GDIs of heterotrimeric G-protein α subunits. *Int. J. Biol. Sci.* **1,** 51–66
14. Chen, C.-K., Eversole-Cire, P., Zhang, H., Mancino, V., Chen, Y.-J., He, W., Wensel, T. G., and Simon, M. I. (2003) Instability of GGL domain-containing RGS proteins in mice lacking the G protein β-subunit Gβ5. *Proc. Natl. Acad. Sci. U.S.A.* **100,** 6604–6609
15. Cheever, M. L., Snyder, J. T., Gershburg, S., Siderovski, D. P., Harden, T. K., and Sondek, J. (2008) Crystal structure of the multifunctional Gβ5-RGS9 complex. *Nat. Struct. Mol. Biol.* **15,** 155–162

16. Martemyanov, K. A., Yoo, P. J., Skiba, N. P., and Arshavsky, V. Y. (2005) R7BP, a novel neuronal protein interacting with RGS proteins of the R7 family. *J. Biol. Chem.* **280,** 5133–5136
17. Drenan, R. M., Doupnik, C. A., Boyle, M. P., Muglia, L. J., Huettner, J. E., Linder, M. E., and Blumer, K. J. (2005) Palmitoylation regulates plasma membrane-nuclear shuttling of R7BP, a novel membrane anchor for the RGS7 family. *J. Cell Biol.* **169,** 623–633
18. Orlandi, C., Posokhova, E., Masuho, I., Ray, T. A., Hasan, N., Gregg, R. G., and Martemyanov, K. A. (2012) GPR158/179 regulate G protein signaling by controlling localization and activity of the RGS7 complexes. *J. Cell Biol.* **197,** 711–719
19. Sandiford, S. L., and Slepak, V. Z. (2009) The Gβ5-RGS7 complex selectively inhibits muscarinic M3 receptor signaling via the interaction between the third intracellular loop of the receptor and the DEP domain of RGS7. *Biochemistry* **48,** 2282–2289
20. Hu, G., and Wensel, T. G. (2002) R9AP, a membrane anchor for the photoreceptor GTPase accelerating protein, RGS9-1. *Proc. Natl. Acad. Sci. U.S.A.* **99,** 9755–9760
21. Zheng, M., Cheong, S.-Y., Min, C., Jin, M., Cho, D.-I., and Kim, K.-M. (2011) β-Arrestin2 plays permissive roles in the inhibitory activities of RGS9-2 on G protein-coupled receptors by maintaining RGS9-2 in the open conformation. *Mol. Cell. Biol.* **31,** 4887–4901
22. Jia, L., Linder, M. E., and Blumer, K. J. (2011) $G_{i/o}$ signaling and the palmitoyltransferase DHHC2 regulate palmitate cycling and shuttling of RGS7 family-binding protein. *J. Biol. Chem.* **286,** 13695–13703
23. Jia, L., Chisari, M., Maktabi, M. H., Sobieski, C., Zhou, H., Konopko, A. M., Martin, B. R., Mennerick, S. J., and Blumer, K. J. (2014) A mechanism regulating G protein-coupled receptor signaling that requires cycles of protein palmitoylation and depalmitoylation. *J. Biol. Chem.* **289,** 6249–6257
24. Panicker, L. M., Zhang, J.-H., Posokhova, E., Gastinger, M. J., Martemyanov, K. A., and Simonds, W. F. (2010) Nuclear localization of the G protein β5/R7-regulator of G protein signaling protein complex is dependent on R7 binding protein. *J. Neurochem.* **113,** 1101–1112
25. Patikoglou, G. A., and Koelle, M. R. (2002) An N-terminal region of *Caenorhabditis elegans* RGS proteins EGL-10 and EAT-16 directs inhibition of $G\alpha_o$ versus $G\alpha_q$ signaling. *J. Biol. Chem.* **277,** 47004–47013
26. Kozasa, T., Hajicek, N., Chow, C. R., and Suzuki, N. (2011) Signalling mechanisms of RhoGTPase regulation by the heterotrimeric G proteins G12 and G13. *J. Biochem.* **150,** 357–369
27. Shu, F. J., Ramineni, S., and Hepler, J. R. (2010) RGS14 is a multifunctional scaffold that integrates G protein and Ras/Raf MAP kinase signalling pathways. *Cell. Signal.* **22,** 366–376
28. Huang, J., Stewart, A., Maity, B., Hagen, J., Fagan, R. L., Yang, J., Quelle, D. E., Brenner, C., and Fisher, R. A. (2014) RGS6 suppresses Ras-induced cellular transformation by facilitating Tip60-mediated Dnmt1 degradation and promoting apoptosis. *Oncogene* **33,** 3604–3611
29. Liu, Z., and Fisher, R. A. (2004) RGS6 interacts with DMAP1 and DNMT1 and inhibits DMAP1 transcriptional repressor activity. *J. Biol. Chem.* **279,** 14120–14128
30. Tayou, J., Wang, Q., Jang, G.-F., Pronin, A. N., Orlandi, C., Martemyanov, K. A., Crabb, J. W., and Slepak, V. Z. (2016) Regulator of G-protein signaling 7 (RGS7) can exist in a homo-oligomeric form that is regulated by $G\alpha_o$ and R7-binding protein. *J. Biol. Chem.* **291,** 9133–9147
31. Orlandi, C., Xie, K., Masuho, I., Fajardo-Serrano, A., Lujan, R., and Martemyanov, K. A. (2015) Orphan receptor GPR158 is an allosteric modulator of regulator of G protein signaling 7 (RGS7) catalytic activity with essential role in dictating its expression and localization in the brain. *J. Biol. Chem.* **290,** 13622–13639
32. Gloeckner, C. J., Boldt, K., Schumacher, A., and Ueffing, M. (2009) Tandem affinity purification of protein complexes from mammalian cells by the Strep/FLAG (SF)-TAP tag. *Methods Mol. Biol.* **564,** 359–372
33. Misra, R. P., and Duncan, S. A. (2002) Gene targeting in the mouse: advances in introduction of transgenes into the genome by homologous recombination. *Endocrine* **19,** 229–238
34. Borchelt, D. R., Davis, J., Fischer, M., Lee, M. K., Slunt, H. H., Ratovitsky, T., Regard, J., Copeland, N. G., Jenkins, N. A., Sisodia, S. S., and Price, D. L. (1996) A vector for expressing foreign genes in the brains and hearts of transgenic mice. *Genet. Anal.* **13,** 159–163
35. Luker, K. E., Smith, M. C., Luker, G. D., Gammon, S. T., Piwnica-Worms, H., and Piwnica-Worms, D. (2004) Kinetics of regulated protein-protein interactions revealed with firefly luciferase complementation imaging in cells and living animals. *Proc. Natl. Acad. Sci. U.S.A.* **101,** 12288–12293
36. Villalobos, V., Naik, S., Bruinsma, M., Dothager, R. S., Pan, M. H., Samrakandi, M., Moss, B., Elhammali, A., and Piwnica-Worms, D. (2010) Dual-color click beetle luciferase heteroprotein fragment complementation assays. *Chem. Biol.* **17,** 1018–1029
37. Hughes, T. E., Zhang, H., Logothetis, D. E., and Berlot, C. H. (2001) Visualization of a functional $G\alpha_q$-green fluorescent protein fusion in living cells. Association with the plasma membrane is disrupted by mutational activation and by elimination of palmitoylation sites, but not by activation mediated by receptors or AlF_4^-. *J. Biol. Chem.* **276,** 4227–4235
38. Katoh, H., Aoki, J., Yamaguchi, Y., Kitano, Y., Ichikawa, A., and Negishi, M. (1998) Constitutively active $G\alpha_{12}$, $G\alpha_{13}$, and $G\alpha_q$ induce Rho-dependent neurite retraction through different signaling pathways. *J. Biol. Chem.* **273,** 28700–28707
39. Kranenburg, O., Poland, M., van Horck, F. P., Drechsel, D., Hall, A., and Moolenaar, W. H. (1999) Activation of RhoA by lysophosphatidic acid and Gα12/13 subunits in neuronal cells: induction of neurite retraction. *Mol. Biol. Cell.* **10,** 1851–1857
40. Sayas, C. L., Avila, J., and Wandosell, F. (2002) Glycogen synthase kinase-3 is activated in neuronal cells by Gα12 and Gα13 by Rho-independent and Rho-dependent mechanisms. *J. Neurosci.* **22,** 6863–6875
41. Moers, A., Nürnberg, A., Goebbels, S., Wettschureck, N., and Offermanns, S. (2008) Gα12/Gα13 deficiency causes localized overmigration of neurons in the developing cerebral and cerebellar cortices. *Mol. Cell. Biol.* **28,** 1480–1488
42. Nürnberg, A., Braüer, A. U., Wettschureck, N., and Offermanns, S. (2008) Antagonistic regulation of neurite morphology through G_q/G_{11} and G_{12}/G_{13}. *J. Biol. Chem.* **283,** 35526–35531
43. Yamazaki, J., Katoh, H., and Negishi, M. (2008) Lysophosphatidic acid and thrombin receptors require both Gα12 and Gα13 to regulate axonal morphology in hippocampal neurons. *Biol. Pharm. Bull.* **31,** 2216–2222
44. Sun, Y., Kim, N. H., Yang, H., Kim, S. H., and Huh, S. O. (2011) Lysophosphatidic acid induces neurite retraction in differentiated neuroblastoma cells via GSK-3β activation. *Mol. Cells* **31,** 483–489
45. Choi, J. W., and Chun, J. (2013) Lysophospholipids and their receptors in the central nervous system. *Biochim. Biophys. Acta.* **1831,** 20–32
46. Bhattacharyya, R., Banerjee, J., Khalili, K., and Wedegaertner, P. B. (2009) Differences in Gα12- and Gα13-mediated plasma membrane recruitment of p115-RhoGEF. *Cell. Signal.* **21,** 996–1006
47. Jordan, J. D., He, J. C., Eungdamrong, N. J., Gomes, I., Ali, W., Nguyen, T., Bivona, T. G., Philips, M. R., Devi, L. A., and Iyengar, R. (2005) Cannabinoid receptor-induced neurite outgrowth is mediated by Rap1 activation through $G\alpha_{o/i}$-triggered proteasomal degradation of Rap1GAPII. *J. Biol. Chem.* **280,** 11413–11421
48. He, J. C., Gomes, I., Nguyen, T., Jayaram, G., Ram, P. T., Devi, L. A., and Iyengar, R. (2005) The $G\alpha_{o/i}$-coupled cannabinoid receptor-mediated neurite outgrowth involves Rap regulation of Src and Stat3. *J. Biol. Chem.* **280,** 33426–33434
49. Drenan, R. M., Doupnik, C. A., Jayaraman, M., Buchwalter, A. L., Kaltenbronn, K. M., Huettner, J. E., Linder, M. E., and Blumer, K. J. (2006) R7BP augments the function of RGS7-Gβ_5 complexes by a plasma membrane-targeting mechanism. *J. Biol. Chem.* **281,** 28222–28231
50. Zhou, H., Chisari, M., Raehal, K. M., Kaltenbronn, K. M., Bohn, L. M., Mennerick, S. J., and Blumer, K. J. (2012) GIRK channel modulation by assembly with allosterically regulated RGS proteins. *Proc. Natl. Acad. Sci. U.S.A.* **109,** 19977–19982
51. Masuho, I., Xie, K., and Martemyanov, K. A. (2013) Macromolecular composition dictates receptor and G protein selectivity of regulator of G protein signaling (RGS) 7 and 9-2 protein complexes in living cells. *J. Biol. Chem.* **288,** 25129–25142
52. Neubig, R. R. (2015) RGS-insensitive G proteins as *in vivo* probes of RGS function. *Prog. Mol. Biol. Transl. Sci.* **133,** 13–30

53. Anderson, G. R., Semenov, A., Song, J. H., and Martemyanov, K. A. (2007) The membrane anchor R7BP controls the proteolytic stability of the striatal specific RGS protein, RGS9-2. *J. Biol. Chem.* **282,** 4772–4781
54. Deleted in proof
55. Nini, L., Waheed, A. A., Panicker, L. M., Czapiga, M., Zhang, J.-H., and Simonds, W. F. (2007) R7-binding protein targets the G protein β5/R7-regulator of G protein signaling complex to lipid rafts in neuronal cells and brain. *BMC Biochem.* **8,** 18
56. Blazer, L. L., Roman, D. L., Chung, A., Larsen, M. J., Greedy, B. M., Husbands, S. M., and Neubig, R. R. (2010) Reversible, allosteric small-molecule inhibitors of regulator of G protein signaling proteins. *Mol. Pharmacol.* **78,** 524–533
57. Popov, S. G., Krishna, U. M., Falck, J. R., and Wilkie, T. M. (2000) Ca^{2+}/calmodulin reverses phosphatidylinositol 3,4,5-trisphosphate-dependent inhibition of regulators of G protein-signaling GTPase-activating protein activity. *J. Biol. Chem.* **275,** 18962–18968
58. Zhang, J. H., and Simonds, W. F. (2000) Copurification of brain G-protein β5 with RGS6 and RGS7. *J. Neurosci.* **20,** RC59
59. Morgans, C. W., Liu, W., Wensel, T. G., Brown, R. L., Perez-Leon, J. A., Bearnot, B., and Duvoisin, R. M. (2007) Gβ5-RGS complexes co-localize with mGluR6 in retinal ON-bipolar cells. *Eur. J. Neurosci.* **26,** 2899–2905
60. Gloeckner, C. J., Boldt, K., Schumacher, A., Roepman, R., and Ueffing, M. (2007) A novel tandem affinity purification strategy for the efficient isolation and characterisation of native protein complexes. *Proteomics* **7,** 4228–4234
61. Klarenbeek, J., Goedhart, J., van Batenburg, A., Groenewald, D., and Jalink, K. (2015) Fourth-generation Epac-based FRET sensors for cAMP feature exceptional brightness, photostability and dynamic range: characterization of dedicated sensors for FLIM, for ratiometry and with high affinity. *PLoS One* **10,** e0122513

Regulation of neurite morphogenesis by interaction between R7 regulator of G protein signaling complexes and G protein subunit G α_{13}

Stephanie L. Scherer, Matthew D. Cain, Stanley M. Kanai, Kevin M. Kaltenbronn and Kendall J. Blumer

J. Biol. Chem. 2017, 292:9906-9918.
doi: 10.1074/jbc.M116.771923 originally published online April 21, 2017
